Accepted Manuscript

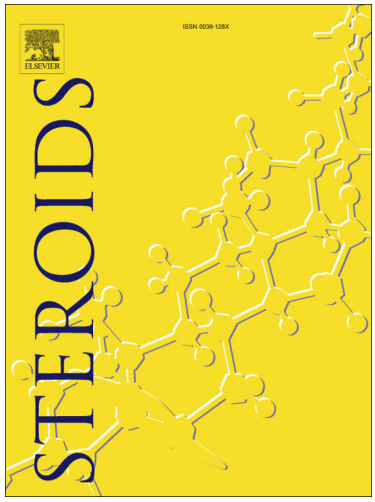

COMPARISON OF [17(20)*E*]-21-NORPREGNENE OXAZOLINYL AND BENZOXAZOLYL DERIVATIVES AS INHIBITORS OF CYP17A1 ACTIVITY AND PROSTATE CARCINOMA CELLS GROWTH

Vladimir A. ZOLOTTSEV, Yaroslav V. TKACHEV, Alexandra S. LATYSHEVA, Vladimir A. KOSTIN, Roman A. NOVIKOV, Vladimir P. TIMOFEEV, Galina E. MOROZEVICH, Alexey V. KUZIKOV, Victoria V. SHUMYANTSEVA, Alexander Y. MISHARIN

PII: S0039-128X(17)30219-2
DOI: https://doi.org/10.1016/j.steroids.2017.11.009
Reference: STE 8191

To appear in: *Steroids*

Received Date: 25 August 2017
Revised Date: 9 November 2017
Accepted Date: 15 November 2017

Please cite this article as: ZOLOTTSEV, V.A., TKACHEV, Y.V., LATYSHEVA, A.S., KOSTIN, V.A., NOVIKOV, R.A., TIMOFEEV, V.P., MOROZEVICH, G.E., KUZIKOV, A.V., SHUMYANTSEVA, V.V., MISHARIN, A.Y., COMPARISON OF [17(20)*E*]-21-NORPREGNENE OXAZOLINYL AND BENZOXAZOLYL DERIVATIVES AS INHIBITORS OF CYP17A1 ACTIVITY AND PROSTATE CARCINOMA CELLS GROWTH, *Steroids* (2017), doi: https://doi.org/10.1016/j.steroids.2017.11.009

COMPARISON OF [17(20)*E*]-21-NORPREGNENE OXAZOLINYL AND BENZOXAZOLYL DERIVATIVES AS INHIBITORS OF CYP17A1 ACTIVITY AND PROSTATE CARCINOMA CELLS GROWTH

Vladimir A. ZOLOTTSEV[1], Yaroslav V. TKACHEV[2], Alexandra S. LATYSHEVA[1], Vladimir A. KOSTIN[1], Roman A. NOVIKOV[2], Vladimir P. TIMOFEEV[2], Galina E. MOROZEVICH[1], Alexey V. KUZIKOV[1], Victoria V. SHUMYANTSEVA[1], and Alexander Y. MISHARIN[1]

[1]Orekhovich Institute of Biomedical Chemistry, Moscow, Russia

[2]Engelhardt Institute of Molecular Biology RAS, Moscow, Russia

Keywords: [17(20)*E*]-21-norpregnene derivatives; CYP17A1 inhibitors; molecular dynamics; PC-3 and LNCaP prostate carcinoma cells; structure-activity relationships.

potency to inhibit 17α-hydroxylase/17,20-lyase (CYP17A1) activity. Among new compounds, the only oxazolinyl derivative comprising 5-oxo-4,5-seco-3-yn- moiety potently inhibited CYP17A1. Binding modes of the oxazolinyl derivatives of [17(20)*E*]-21-norpregnene were analyzed by molecular dynamics simulations, and model of alternate, water-bridged type II interaction was proposed for these compounds. Eight new compounds, together with two CYP17A1-inhibiting oxazolinyl derivatives synthesized earlier, abiraterone and galeterone were evaluated for their potency to inhibit prostate carcinoma PC-3 and LNCaP cells growth. Oxazolinyl and benzoxazolyl derivatives comprising 3β-hydroxy-5-ene moieties potently inhibited prostate carcinoma cell growth; inhibitory potencies of 3-oxo-4-en- and 5-oxo-4,5-seco-3-yn- derivatives were significantly lower.

CYP17A1 inhibitor – 17-(3-pyridyl)-androsta-5,16-dien-3β-ol (abiraterone) [6] – has been approved for treatment of prostate cancer in clinical setting. Besides inhibition of CYP17A1, abiraterone elicits antitumor activity by blocking some downstream enzymes of the steroid pathway [7]; competitively antagonizing subsequent androgen receptor signaling [8,9]; decreasing cell growth and proliferation (associated with DNA fragmentation and pro-apoptotic modulation of p21, caspase-3, survivin, and transforming growth factor β [10]).

Another CYP17A1 inhibitor – 3β-(hydroxy)-17-(1H-benzimidazole-1-yl)androsta-5,16-diene (galeterone) [11] – is under stage 3 of clinical trials for treatment of castration resistant prostate cancer. The size and structure of azole substituent strongly affects the inhibitory potency and other biological activities of these compounds: galeterone was 150-fold less potent than abiraterone as CYP17A1 inhibitor, however, it was found also to be potent androgen receptor antagonist and degrading agent, and induced endoplasmic reticulum stress response [12-15].

Effects of abiraterone and galeterone in cultured prostate carcinoma cells, particularly in androgen-dependent LNCaP and androgen-independent PC-3 cells, are well documented. Both abiraterone and galeterone inhibit growth and proliferation of LNCaP and PC-3 cells in a time- and dose-dependent manner, down-regulate expression of PSA and mutant androgen receptor (T877A), and suppress androgens biosynthesis in LNCaP cells [9,10,13-15].

Data reported so far indicate that some nitrogen-containing derivatives of [17(20)*E*]-pregnene may also be considered as promising candidates for the development of new cancer treatment agents. Some 17(*E*)-picolinylidene androstene derivatives inhibited CYP17A1, decreased growth, proliferation and induced apoptosis in breast and prostate carcinoma cells [16-18]; oxazolinyl derivatives of [17(20)*E*]-21-norpregnene **1** and **2** (Figure 1) suppressed catalytic activity of recombinant human CYP17A1 as potently as abiraterone [19,20].

Continuing investigation of derivatives of [17(20)*E*]-pregnene in the present study we have synthesized four new oxazolines **3 - 6**, and four new benzoxazoles **7 – 10** (Figure 1). Since the inhibitory potency of oxazolinyl derivatives of [17(20)*E*]-21-norpregnene towards CYP17A1 apparently was dependent on their structure in a specific manner, we evaluated biological activity of the new oxazolines **3**, **4**, **5** (lacking hydroxyl- or keto- substituent at C-3) and **6** (comprising truncated steroid backbone), as well as related compounds **7 – 10** (comprising bulky benzoxazole substituent, instead of oxazoline).

2. EXPERIMENTAL

2.1. MATERIALS AND GENERAL METHODS

Melting points were measured in glass capillaries; HRMS were registered on a Bruker 'Apex Ultra' FT ICR MS instrument in ion-positive electrospray ionization mode; ^{1}H NMR and ^{13}C NMR spectra – on an AMX-III instrument (Bruker, 400 MHz) in $CDCl_3$ (chemical shift of residual solvent protons was 7.25 ppm, of ^{13}C in $CDCl_3$ - 77.16 ppm). Flash chromatography was performed on (0.035 – 0.070 mm) silica gel from 'Acros', TLC – on Silica gel UV-254 HPTLC plates and UV-254 PTLC plates from 'Merck'.

Abiraterone was purchased from 'ChemLeader Ltd' (Shanghai, China), galeterone – from 'Selleck'; recombinant CYP17A1 [21] was obtained from Institute of Bioorganic Chemistry of National Academy of Sciences of Belarus (Minsk, Belarus). Pregnenolone, didodecyldimethyl ammonium bromide (DDAB), and Triton X 100 were purchased from 'Sigma'. 2'-{[(*E*)-3β-Hydroxyandrost-5-en-17-ylidene]methyl}-4',5'-dihydro-1',3'-oxazole **1**, 2'-{[(*E*)-3-oxoandrost-4-en-17-ylidene]methyl}-4',5'-dihydro-1',3'-oxazole **2**, [17(20)*E*]-3β-acetoxy-pregna-5,17(20)-dien-21-oic acid **18**, [17(20)*E*]-3-oxopregna-4,17(20)-dien-21-oic acid **19**, ethyl [17(20)*E*]-3β-*p*-toluenesulfonyloxypregna-5,17(20)-dien-21-oate **11**, and ethyl [17(20)*E*]-3-oxopregna-4,17(20)-dien-21-oate **14** were synthesized as reported earlier [20], other reagents and solvents were purchased from 'Aldrich', 'Merck', and 'Acros'.

Three-pronged screen-printed graphite (graphite printing pasta Achison, USA) working and auxiliary electrodes (AVTOKOM, Russia, http://www.membranes_moscow.ru), and a reference silver/silver chloride Ag/AgCl electrode were used in this study. Diameter of the working electrode surface was 2 mm.

2.2. CHEMICAL SYNTHESIS

2.2.1. Methyl [17(20)E]-6β-methoxy-3α,5α-cyclopregn-17(20)-en-21-oate **12**

Tosylate **11** (1.025 g, 2 mmol) was added to boiling solution of CH_3COONa (0.82 g, 10 mmol) in abs. methanol (60 mL), then the mixture was heated under reflux for 3 h, cooled, and evaporated. The residue was treated with benzene (100 mL) and water (50 mL); the benzene extract was washed with brine (30 mL), dried over Na_2SO_4 and evaporated. Compound **12** was isolated as colorless glass (610 mg, 1.7 mmol, 85%) by silica gel flash chromatography in

46.6, 48.3, 50.9; 53.8, 56.7 (C9, C10, C13, C14, C6-O$\underline{CH_3}$, C21-O$\underline{CH_3}$); 82.3 (C6); 108.0 (C20); 168.0 (C17); 177.0 (C21).

***2.2.2. [17(20)E]-6β-Methoxy-3α,5α-cyclopregn-17(20)-en-21-oic acid* 13**

Methyl ester **12** (537 mg, 1.5 mmol), 4M aqueous NaOH solution (1.2 mL) and *iso*-propanol (10 mL), was stirred and heated under reflux until the hydrolysis was complete according to TLC (~ 3 h), then the mixture was acidified with diluted aqueous HCl to pH 2 and extracted with ethyl acetate (4 X 15 mL). Extract was dried over anhydrous Na_2SO_4, evaporated, and the residue was purified by silica gel flash chromatography in hexane:ethyl acetate:CH_3COOH (75 : 24 : 1) mixture to obtain acid **13** (405 mg, 1.17 mmol, 78 %) as white solid. HRMS, calculated for $[C_{22}H_{33}O_3]^+$: 345.2430; found: 345.2217; ^{1}H NMR: 0.43 and 0.66 (each 1H, m, H-4); 0.88 (3H, s, H-18); 1.04 (3H, s, H-19); 2.74-2.89 (3H, m, H-6 and H-16); 3.33 (3H, s, CH_3O); 5.54 (1H, t, J = 2.3 Hz, H-20); ^{13}C NMR: 13.3 (C4); 18.7, 19.4; 21.5, 22.7, 24,4, 25.0 (C2, C3, C4, C15, C18, C19); 30.4, 30.9, 33.5, 34.4, 35,2, 35.6 (C1, C5, C7, C8, C12, C16) ; 43.6, 48.3; 51.2, 53.7, 56.7 (C9, C10, C13, C14, C6-O$\underline{CH_3}$); 82.3 (C6); 107.9 (C20); 172.24 (C17) 179.8 (C21).

***2.2.3. Ethyl [17(20)E]-3-oxo-4,5-epoxypregn-17(20)-en-21-oate* 15**

Ethyl [17(20)*E*]-3-oxopregna-4,17(20)-dien-21-oate **14** (1.43 g, 4 mmol) was dissolved in methanol (40 mL), the solution was cooled to 4^{o}C, then aqueous 30% hydrogen peroxide (4.8 mL) and aqueous 4M NaOH (4.0 mL) were added, and the mixture was stirred at 4^{o}C for 18 h. Thereafter the mixture was poured into mixture of 10% $Na_2S_2O_3$ solution (150 mL) and chopped ice (50 g), neutralized with 5% aqueous HCl. The white precipitate was separated, washed with water and dried to obtain crude epoxide **15** (1.24 g, 3.32 mmol, 83 %) as mixture of related 4α,5α- and 4β,5β- isomers in a ratio of 3:1. Analytical sample was purified by silica gel flash chromatography in hexane:acetone (7:1) mixture. HRMS, calculated for $[C_{23}H_{33}O_4]^+$: 373.2379; found: 373.2376; ^{1}H NMR for 4α,5α-isomer : 0.84 (3H, s, H-18); 1.16 (3H, s, H-19); 1.27 (3H, t, J = 7.2 Hz, ethyl); 2.97 (1H, s, H-4); 4.13 (2H, q, J = 7.2 Hz, ethyl); 5.51 (1H, t, J = 2.5 Hz, H-20); ^{1}H NMR for 4β,5β-isomer: ^{1}H NMR: 0.85 (3H, s, H-18); 1.07 (3H, s, H-19); 1.27 (3H, t, J = 7.2 Hz, ethyl); 3.04 (1H, s, H-4); 4.13 (2H, q, J = 7.2 Hz, ethyl); 5.53 (1H, t, J = 2.5 Hz, H-20).

the consequent formation and degradation of related tosyl hydrazone being monitored by TLC. The mixture was then diluted with dichloromethane (50 mL) and neutralized with excess of $NaHCO_3$. Then water (50 mL) was added, dichloromethane layer was separated, the aqueous layer was extracted with dichloromethane (2 X 25 mL); the combined extract was washed with brine (20 mL), dried over Na_2SO_4 and evaporated. 4,5-Secosteroid **16** (440 mg 1.24 mmol, 62 %) was isolated by silica gel flash chromatography in hexane:ethyl acetate (3:1) mixture as colorless glass. HRMS, calculated for $[C_{23}H_{33}O_3]^+$: 357.2430; found: 357.2431; ^{1}H NMR: 0.88 (3H, s, H-18); 1.10 (3H, s, H-19); 1.27 (3H, t, J = 7.2 Hz, ethyl); 1.92(1H, t, J = 2.3 Hz, H-4); 4.14 (2H, q, J = 7.2 Hz, ethyl); 5.54 (1H, t, J = 2.5 Hz; H-20); ^{13}C NMR: 13.9, 14.4, 18.6, 20.5, 21.6, 24.5 (C2, C11, C15, C18, C19, OCH_2-$\underline{CH_3}$); 30.3, 30.9, 33.6, 34.7, 38.0, 46.2 (C1, C6, C7, C8, C12, C16); 47.6, 50.9, 53.0; 55.8 (C9, C10, C13, C14); 59.7 (OCH_2-CH_3); 68.2 (C4); 86.0 (C3); 109.1 (C20); 167.36 (C17); 175.1 (C21); 214.1 (C5).

***2.2.5. [17(20)E]-4,5-seco-5-oxopregn-17(20)-en-3-yn-21-oic acid* 17.**

Ethyl ester **16** (425 mg, 1.2 mmol), 4M aqueous NaOH solution (1.2 mL) and *iso*-propanol (10 mL), was stirred and heated under reflux until the hydrolysis was complete according to TLC (~ 3.5 h), then the mixture was acidified with diluted aqueous HCl to pH 2 and extracted with ethyl acetate (4 X 15 mL). Extract was dried over anhydrous Na_2SO_4, evaporated, and the residue was purified by silica gel flash chromatography in hexane:ethyl acetate:CH_3COOH (75 : 24 : 1) mixture to obtain 4,5-secoacid **17** (308 mg, 0.94 mmol, 78 %) as white solid. HRMS, calculated for $[C_{21}H_{29}O_3]^+$: 329.2117; found: 329.2111; ^{1}H NMR: 0.89 (3H, s, H-18); 1.10 (3H, s, H-19); 1,92 (1H, t, 2.3 Hz, H-4); 2.86 (2H, m, H-16); 5.56 (1H, t, J = 2.5 Hz, H-20); ^{13}C NMR: 13.8, 18.4, 20.6, 21.5, 24.3 (C2, C11, C15, C18, C19); 29.7, 30.6, 30.8, 33.5, 34.6, 37.9 (C1, C6, C7, C8, C12, C16); 46.6, 47.6, 51.0, 53.0 (C9, C10, C13, C14); 68.3 (C4); 85.1 (C3); 108.8 (C20); 172.5 (C17); 178.30 (C21); 214.2 (C5).

***2.2.6. Procedure for preparation of oxazolines* 3 *and* 6.**

Stirred mixture of acid (**13** or **17,** 0.5 mmol), triphenyl phosphine (524 mg, 2 mmol) and dry CH_3CN (5 mL) was cooled to +2^{o}C, then mixture of CCl_4 (0.46 mL, 5 mmol) and CH_3CN (2 mL) was added by drops at +2^{o}C during 10 min. The resulting mixture was stirred for 2 h at

hydrochloride, diluted with benzene (40 mL), washed with saturated K_2CO_3 solution (10 mL), then with brine (20 mL), dried over Na_2SO_4, and evaporated. Isolation of the obtained oxazolines was performed as indicated below.

***2.2.7. 2'-{[(E)-6β-Methoxy-3α,5α-cycloandrostan-17-ylidene]methyl}-4',5'-dihydro-1',3'-oxazole* 3.**

Compound **3** (113 mg, 0.31 mmol, 62 %) was obtained by silica gel flash chromatography in hexane:acetone (5 : 1) mixture. HRMS calculated for $[C_{24}H_{36}NO_2]^+$: 370.2746; found: 370,2734; ^{1}H NMR: 0.43 and 0.66 (each 1H, m, H-4) 0.86 (3H, s, H-18); 1.03 (3H, s, H-19); 2.69 – 2.51 (3H, m, H-6 and H-16); 3.32 (3H, OCH_3,), 3.88 and 4.22 (each 2H, m, CH_2, oxazoline); 5.62 (1H, t, J = 2.5 Hz, H-20); ^{13}C NMR: 13.2 (C4); 18.9, 19.4, 21.6, 22.8, 24.5, 25.0 (C2, C3, C11, C14, C18, C19); 30.4, 33.5, 35.1, 35.4, 35.9 (C1, C5, C7, C8, C12, C16); 43.6, 46.3, 48.3, 53.9, 54.6, 56.7 (C9, C10, C13, C14, C4', OCH_3); 66.9 (C5'); 82.2 (C6); 105.0 (C20); 165.4 (C2'); 169.5 (C17).

***2.2.8. 2'-{[(E)-4,5-secoandrost-3-yn-5-on-17-ylidene]methyl}-4',5'-dihydro-1',3'-oxazole* 6.**

Crude mixture containing target oxazoline **6** was treated with boiled mixture of toluene:hexane (3 : 4, 20 mL), the solution was stored for 4 h at r. t., and the precipitated triphenyl phosphine oxide was filtered off. The solution was evaporated, and the residue was subjected to silica gel flash chromatography in hexane:*iso*-propanol (6 : 1) mixture, followed by preparative TLC in the same system to obtain oxazoline **6** (85 mg, 0.24 mmol, 48 %) as colorless viscous oil, crystallizing during storage. HRMS calculated for $[C_{23}H_{32}NO_2]^+$: 354.2433; found: 354.2428; ^{1}H NMR: 0.88 (3H, s, H-18); 1.10 (3H, s, H-19); 1.92 (1H, t, J = 2.4 Hz, H-4); 2.76 (2H, m, H-16); 3.91 and 4.25 (each 2H, m, CH_2, oxazoline); 5.64 (1H, t, J = 2.5 Hz, H-20); ^{13}C NMR: 13.9, 18.6, 20.6, 21.6, 24.5 (C2, C11, C15, C18, C19); 30.1, 30.9, 33.6, 34.7, 34.9, 38.0 (C1, C6, C7, C8, C12, C16); 46.0, 47.6, 50.9, 53.2, 54.4 (C9, C10, C13, C14, C4'); 67.0, 68.2 (C4, C5'); 85.0 (C3); 105.6 (C20); 165.3, 168.3 (C17, C2'); 214.21 (C5).

***2.2.9. 2'-{[(E)-3β-Methoxyandrost-5-en-17-ylidene]methyl}-4',5'-dihydro-1',3'-oxazole* 4**

Solution of oxazoline **3** (74 mg, 0.2 mmol) and *p*-toluenesulfonic acid (40 mg, 0.23 mmol) in

$[C_{24}H_{36}NO_2]^+$: 370.2746; found: 370.2741; ^{1}H NMR: 0.82 (3H, s, H-18); 1.01 (3H, s, H-19); 2.74 (1H, m, H-16); 3.05 (1H, m, H-3); 3.34 (3H, OCH_3), 3.88 and 4.22 (each 2H, m, CH_2, oxazoline); 5.35 (1H, m, H-6) 5.66 (1H, br. t, J ≈ 2.3 Hz, H-20); ^{13}C NMR: 18.4, 19.5, 21.1, 24.6 (C11, C15, C18, C19); 28.1, 30.3, 31.8(x2), 35.4, 37.1, 37.3, 38.8 (C1, C2, C4, C7, C8, C10, C12, C16) ; 45.9; 50.5, 54.2, 54.5, 55.7 (C9, C13, C14, C4', OCH_3); 66.9 (C5'); 80.36 (C3); 105.2(C20); 121.3 (C6); 141.1 (C5); 165.4 (C2'); 169.3 (C17).

***2.2.10. 2'-{[(E)-3β-Chloroandrost-5-en-17-ylidene]methyl}-4',5'-dihydro-1',3'-oxazole* 5**

Oxazoline **3** (70 mg, 0.2 mmol) was dissolved in 1M solution of HCl in tetrahydrofurane (2 mL), the solution was stored for 2 h at r. t., and then evaporated to dryness. The residue was treated with $CHCl_3$ (15 mL), and saturated $NaHCO_3$ solution (5 mL), chloroform layer was washed with brine (15 mL), dried over Na_2SO_4, and evaporated. The residue was separated by silica gel flash chromatography in hexane:*iso*-propanol (8 : 1) mixture, followed by evaporation, to obtain compound **5** (62 mg, 0.17 mmol, 83 %) as white solid film. HRMS calculated for $[C_{23}H_{33}ClNO]^+$: 374.2251; found: 374.2250; ^{1}H NMR: 0.82 (3H, s, H-18); 1.04 (3H, s, H-19); 2.75 (1H, m, H-16); 3.89 (1H, m, H-3); 3.89 and 4.24 (each 2H, m, CH_2, oxazoline); 5.37 (1H, m, H-6); 5.66 (1H, br. t, J ≈ 2.3 Hz, H-20); ^{13}C NMR: 18.4, 19.4, 21.0, 24.6 (C11, C15, C18, C19); 29.8, 30.3, 31.6, 31.7, 33.4, 35.4, 36.6 (C1, C2, C7, C8, C10, C12, C16); 39.2, 43.5, 50.3 (C4, C9, C13); 54.1, 54.3, 60.2 (C3, C14, C4'); 67.0 (C5'); 105.2 (C20); 121.4 (C6), 141.0 (C5); 163.2 (C2'); 165.6 (C17).

***2.2.11. Procedure for preparation of benzoxazoles* 7 -10**

Stirred mixture of carboxylic acid (**13, 17, 18, 19,** 0.5 mmol), triphenyl phosphine (524 mg, 2 mmol) and dry CH_3CN (6 mL) was cooled to +2^{o}C, then mixture of CCl_4 (483 µL, 5 mmol) and dry CH_3CN (1 mL) was added by drops at +2^{o}C. The resulting mixture was stirred at +2^{o}C for 90 min, until clear solution formed. Solution of *o*-aminophenol (71 mg, 0.65 mmol) and dry pyridine (200 µL, 2.5 mmol) in 1 mL of dry CH_3CN was added by drops at +2^{o}C, and the mixture was stirred at +2^{o}C for 10 min, then at 20^{o}C for 20 min. Formation of intermediate amide was proved by ^{1}H-NMR and HRMS analysis of aliquots picked up from the reaction mixture. (For *17(20)E1-3β-acetoxy-21-[(2-hydroxyphenyl)-2-amino]-21-oxopregna-5,17(20)*

was dissolved in $CHCl_3$ (25 mL), treated with $NaHCO_3$ saturated solution (10 mL), chloroform layer was washed with brine (10 mL), dried over Na_2SO_4, and evaporated to dryness. Isolation of the obtained benzoxazoles was performed as indicated below.

***2.2.12. 2'-{[(E)-3β-Hydroxyandrost-5-en-17-ylidene]methyl}-benzo-[d]-oxazole* 7(*E*)**

Residue containing crude benzoxazole was separated by silica gel flash chromatography in hexane:ethyl acetate (4:1) to obtain compound **18a** (mixture of two products at 3 : 1 ratio, 143 mg, 0.32 mmol, 64%) as light beige solid. HRMS, calculated for $[C_{29}H_{36}NO_3]^+$: 446.2695; found: 446.2695. ^{1}H NMR for major product: 0.92 and 1.06 (each 3H, s, H-18 and H-19); 6.17 (1H, t, J≈2.0 Hz, H-20); ^{1}H NMR for minor product: 1.07 and 1.19 (each 3H, s, H-18 and H-19); 6.20 (1H, t, J≈2.0 Hz, H-20). Pure *E*-isomer **18a(*E*)** was isolated by preparative TLC in hexane:ethyl acetate (4:1) mixture (93 mg, 0.21 mmol, 42%). ^{1}H NMR: 0.92 (3H, s, H-18); 1.06 (3H, s, H-19); 2.02 (3H, s, Ac); 3.02 (2H, m, H-16); 4.61 (1H, m, H-3); 5.40 (1H, m, H-6); 6.17 (1H, t, J=2.0 Hz, H-20); 7.27 (2H, m, aryl), 7.46 and 7.67 (each 1H, m, aryl). ^{13}C NMR: 18.5, 19.4, 21.1, 21.5, 24.8, 27.9 (C2, C11, C15, C18, C19, CH_3-acetate); 30.9, 31.8, 31.2, 35.4, 36.8, 37.1, 38.2 (C1, C4, C7, C8, C10, C12, C16); 50.3; 54.2, 58.6 (C9, C13, C14); 73.9 (C3); 104.7 (C20); 110.4, 119.5, 119.7, 122.4, 124.6, 124.7, 140.0, 150.2 (C5, C6 and benzoxazole); 163.9 (C2'); 170.0 (C17); 170.7 (CO-acetate). Mixture of acetate **18a(*E*)** (89 mg, 0.2 mmol), K_2CO_3 (500 mg), MeOH (2.5 mL), water (1.5 mL) was heated under reflux for 45 min while stirring, $CHCl_3$ (20 mL) and water (10 mL) were added after cooling, the aqueous layer was extracted with $CHCl_3$ (2 X 10 mL), the combined extract was washed with brine (10 mL), dried over Na_2SO_4, and evaporated, followed by crystallization from methanol to obtain benzoxazole **7(*E*)** (69 mg, 0.17 mmol, 86%) as light beige solid. HRMS, calculated for $[C_{27}H_{34}NO_2]^+$: 404.2584; found: 404.2583. ^{1}H NMR: 0.92 (3H, s, H-18); 1.05 (3H, s, H-19); 3.01 (2H, m, H-16); 3.52 (1H, m, H-3); 5.36 (1H, m, H-6); 6.17 (1H, t, J=2.0 Hz, H-20); 7.46 and 7.67 (each 2H, m, aryl). ^{13}C NMR: 18.5, 19.6, 21.1, 24.8 (C11, C15, C18, C19); 31.0, 31.7, 31.8 (x2) (C2, C7, C8, C16); 35.4, 36.8, 37.4 (C1, C10, C12); 42.4 (C4); 46.4 , 50.4, 54.3 (C4, C9, C13); 71.8 (C3); 104.7 (C20); 110.2, 119.6, 121.4, 124.2, 124.4, 141.0, 142.3, 150.3 (C5, C6 and benzoxazole); 164.0 (C2'); 170.1 (C-17).

as light beige solid. HRMS, calculated for $[C_{27}H_{32}NO_2]$+: 402.2433; found: 402.2432. ^{1}H NMR for major product: 0.96 and 1.23 (each 3H, s, H-18 and H-19); 6.17 (1H, t, J≈2.0 Hz, H-20); ^{1}H NMR for minor product: 0.94 and 1.22 (each 3H, s, H-18 and H-19); 6.19 (1H, t, J≈2.0 Hz, H-20). Pure *E*-isomer **8(*E*)** was isolated by preparative TLC in hexane:ethyl acetate (4:1) mixture, followed by crystallization from methanol (76 mg, 0.19 mmol, 38%). Light beige crystals with m.p. 227-229ºC, ^{1}H NMR: 0.96 (3H, s, H-18); 1.23 (3H, s, H-19); 3.03 (2H, m, H-16); 5.75 (1H, s, H-4); 6.17 (1H, t, J=2.3 Hz, H-20); 7.28 (2H, m, aryl), 7.47 and 7.67 (each 1H, m, aryl). ^{13}C NMR: 17.5; 18.7; 21.1; 24.6 (C18, C19, C-11, C-15); 30.8; 31.9; 32.9; 34.0 (C-16, C-7, C-6, C-2); 35.3; 35.5; 35.8; 38.8 (C-12, C-1, C-8, C-10); 46.3; 53.4; 54.0 (C-13, C-9, C-13); 104.9 (C-20); 110.2; 119.7; 124.2; 124.3; 124.5; 142.3; 150.3; 163.7 (C4, C5 and benzoxazole); 169.3 (C2'); 170.8 (C17); 199.4 (C-3).

2.2.14. 2'-{[(E)-6β-Methoxy-3α,5α-cycloandrostan-17-ylidene]methyl}-benzo-[d]-oxazole 9(E). Crude benzoxazole was purified by silica gel flash chromatography in hexane:ethyl acetate (4:1) mixture to obtain compound **9** (mixture of two products at 3 : 1 ratio, 118 mg, 0.28 mmol, 56 %) as light beige solid. HRMS, calculated for $[C_{28}H_{36}NO_2]^+$: 418.2746; found: 418.2742. ^{1}H NMR for major product: 0.96 and 1.07 (each 3H, s, H-18 and H-19); 6.16 (1H, t, J≈2.0 Hz, H-20); ^{1}H NMR for minor product: 0.92 and 1.04 (each 3H, s, H-18 and H-19); 6.17 (1H, t, J≈2.0 Hz, H-20). Pure *E*-isomer **9(*E*)** was isolated by preparative TLC in hexane:ethyl acetate (4:1) mixture as light beige foam (75 mg, 0.18 mmol, 36%). ^{1}H NMR: 0.46 and 0.67 (each 1H, m, H-4) 0.96 (3H, s, H-18); 1.07 (3H, s, H-19); 2.80 (1H, t, J=2.6 Hz, H-6); 3.01 (2H, m, H-16); 3.35 (3H, s, OCH_3); 6.16 (1H, t, J=2.5 Hz, H-20); 7.27 (2H, m, aryl), 7.46 and 7.66 (each 1H, m, aryl). ^{13}C NMR: 13.3 (C4); 19.0, 19.4, 21.6, 22.8, 24.6, 25.0 (C2, C3, C11, C14, C18, C19); 30.5, 31.0, 33.5, 35.2, 35.4, 35.8 (C1, C5, C7, C8, C12, C16); 43.6, 46.8, 48.3, 54.1, 56.7 (C9, C10, C13, C14, OCH_3); 82.3 (C6); 104.4 (C-20); 110.3, 119.9, 124.2, 124.3, 142.3, 150.3 (benzoxazole); 164.0 (C2'); 170.4 (C-17).

phosphine oxide was filtered off, the solution was evaporated. The residue was separated by silica gel flash chromatography in hexane:ethyl acetate (7 : 2) mixture, followed by purification of the fraction containing benzoxazole **10** (mixture of two products at 3 : 1 ratio) ^{1}H NMR for major product: 0.98 and 1.13 (each 3H, s, H-18 and H-19); 6.18 (1H, t, J≈2.0 Hz, H-20); ^{1}H NMR for minor product: 0.94 and 1.12 (each 3H, s, H-18 and H-19); 6.19 (1H, t, J≈2.0 Hz, H-20). Pure *E*-isomer **10 (*E*)** was obtained by preparative TLC in hexane:ethyl acetate (3 : 1) mixture as light beige foam (56 mg, 0.14 mmol, 28%). HRMS, calculated for $[C_{27}H_{32}NO_2]^+$: 402.2433; found: 402.2418. ^{1}H NMR: 0.98 (3H, s, H-18); 1.13 (3H, s, H-19); 1.93 (1H, t, J = 2.4 Hz, H-4); 3.04 (2H, m, H-16); 6.18 (1H, t, J = 2.3 Hz, H-20); 7.28 (2H, m, aryl), 7.47 and 7.67 (each 1H, m, aryl). ^{13}C NMR: 13.9, 18.7, 20.7, 21.7, 24.7 (C2, C11, C15, C18, C19); 29.8, 30.8, 30.9, 33.7, 34.8, 34.9, 38.1 (C1, C6, C7, C8, C10, C12, C16); 47.6, 51.0, 53.4 (C9, C10, C13, C14); 68.2 (C4); 85.0 (C3); 105.0 (C20); 110.2, 119.7, 124.3, 124.5, 142.3, 150.3 (benzoxazole); 163.7 (C2'); 168.9 (C17); 214.1 (C5).

2.3. ELECTROCHEMICAL MEASUREMENTS

Electrochemical experiments were performed using an AUTOLAB PGSTAT12 potentiostat (EcoChemie) equipped with GPES software. All electrochemical measurements were performed at room temperature in 1 mL of 0.1 M potassium phosphate buffer, pH 7.4, containing 0.05 M NaCl and 0.04% Triton X-100. For preparation of enzyme electrodes, 1 μL of 0.1 M DDAB in chloroform was applied on the surface of a graphite electrode. After evaporation of chloroform (10 min), 1 μL of 15.7 μM CYP17A1 was applied. The enzyme electrodes were then kept at 4ºC for 12 h in a wet chamber to prevent complete electrode drying. Chronoamperometric assays were performed in 1 mL of 0.1 M potassium phosphate buffer, containing 0.05 M NaCl and 0.04% Triton X-100, pH 7.4, at fixed working electrode potential of -0.45 V (vs. Ag/AgCl), and constant stirring. Titration was performed with ethanol solution of pregnenolone, after reaching the steady-state current; concentration of the tested compounds was varied from 1 μM to 30 μM. Inhibitory activities of compounds **3–10** and galeterone were calculated from chronoamperometric titration data, analyzed by the non-linear regression method (electrochemical Michaelis–Menten model equation $I_{ss} = (I_{max}\,[S])/(K_M + [S])$), using OriginPro 7.5 software package.

of CYP17A1 complex with inhibitor abiraterone). Single protein unit and crystallographic water molecules were retained, and abiraterone molecule replaced with one of the two new inhibitors by superimposing steroid cores. Initial ligand conformations were generated by simulated annealing followed by minimization using MMFF94 force field. Two structures were generated for each inhibitor: one containing bound water molecule at 6-th coordinate position of Heme iron, and another with free 6-th coordinate position. Structures were then solvated in water box (90 x 100 x 90 Å), and ions were added at 0.15M concentration to neutralize the system net charge, and mimic physiological ionic strength. Emplaced ligand and generated bulk water molecules were initially minimized, while protein atoms together with bound crystallographic water were kept fixed. Then, the protein Cα atoms were harmonically constrained, and whole system was minimized, heated to 300K and equilibrated for 150 ns at pressure target of 1.01325 bar. Constrains on protein atoms were subsequently gradually released, and production runs of 60 ns were initiated. Equilibrium nature of trajectories was confirmed by root mean square deviation (RMSD) curves not showing significant trends after initial 20 ns (Supplementary data, Figs. S-3, S-7, S-12, S-17). Protein stability was verified by per-residue root mean square fluctuation (RMSF) analysis (Supplementary data, Figs. S-4, S-8, S-13, S-18), where Cα atoms of rigid core residues experienced fluctuations of less than 1Å on RMS average. To avoid possible non-equilibrium effects, initial 20 ns was stripped prior to trajectory analysis.

Force field parameter set for the protein was CHARMM27 with CMAP dihedral correction. Parameters for the ligands were obtained by SwissParam server [22]. Heme partial charges were adopted from [23]. Water model was TIP3p. VMD package [24] was used for initial structure preparation, MD trajectory post-processing, analysis, and visualization. Computations were performed on 8-core Intel(R) Xeon(R) CPU E5-1620 v3 with NVIDIA GPGPU (CUDA) acceleration, and 32-core Intel(R) Xeon(R) CPU E5-2670 workstations. NAMD software [25] was used to perform the simulations using periodical boundary conditions with the Ewald summation method. Plots were produced with Matplotlib Python package [26,27].

densities in RPMI 1640 medium supplemented with 10% fetal calf serum (FCS; Gibco, Grand Island, NY), and 1% penicillin/streptomycin (Gibco) in a 5% CO_2 atmosphere at 37^{o}C for 24 hr. The cells were seeded at 2 X 10^4 cells/well for 48 h, then treated with tested compounds at the designated concentrations, and incubated for an additional 96 h. Effect of compounds on cell growth was examined by MTT assay [28].

Solution of 3-(4,5-dimethylthiazol-2-yl)-2,5-diphenyltetrazolium bromide (MTT, 5 mg/mL) was added, and the cells were incubated for 4 h, followed by absorbance measurement at 570 nm, with 'SpectraMax 190' microplate reader. Viability of treated cells was expressed as a percentage relative to control. Each experiment was performed in triplicate and independently repeated at least four times.

2). Reported earlier tosylate **11** [20] was transformed to compound **12** by treatment with methanol in the presence of CH_3COONa in 85% yield. Formation of 6β-methoxy-3α,5α-cyclo fragment accompanied with transesterification of 21-carboxylic group (additional experiments showed that ethyl esters of pregn-17(20)-en-21-oic acid transformed to related methyl esters under aforementioned conditions). The methyl ester **12** was subjected to alkaline hydrolysis, and obtained acid **13** was introduced into reaction with triphenyl phosphine, carbon tetrachloride, and ethanolamine, in the presence of triethyl amine, to give oxazoline **3** in 62% yield. Oxazolines **4** and **5** were prepared from compound **3** in high yields by acid catalyzed methanolysis, or treatment with HCl in tetrahydrofurane, respectively (Scheme 1).

For preparation of oxazoline **6** comprising seco-A pregnene moiety, ketosteroid **14** [20] was chosen as starting compound. Selective epoxidation of Δ^4 with hydrogen peroxide under alkaline conditions led to compound **15** (mixture of 4α,5α- and 4β,5β- epoxides in a ratio of 2 : 1) in 83% yield, which without separation of isomers was subjected to Eshenmoser fragmentation. Treatment of the compound **15** with *p*-tosyl hydrazine in dichloromethane - acetic acid mixture (3 : 1) led to ethyl ester **16**, which was subjected to alkaline hydrolysis, and the resulted acid **17** was transformed to the oxazoline **6** in 48% yield according the procedure mentioned above.

We have performed a synthesis of benzoxazolyl derivatives **7 - 10** (scheme 3) starting from steroid acids **13**, **17**, **18**, **19**, and *o*-aminophenol, according the procedure used for synthesis of oxazolines, with following modification: the cyclization step was carried out in the presence of pyridine instead of triethyl amine. Preliminary experiments revealed that cyclization of intermediate amides (shown in brackets) in the presence of strong bases gave target benzoxazoles in low yield, and was accompanied by formation of complex mixture of byproducts.

If the cyclization step was conducted in the presence of pyridine at 50°C during 3 h, yield of benzoxazoles **7 - 10** was > 50 %, however, in contrast to synthesis of oxazolines, all these benzoxasoles were obtained as mixtures of two products.

Mechanism of benzoxazole formation was previously investigated [30]. According to this mechanism, amide **A** is in equilibrium with cyclol **B**, which reacts with triphenylphosphine dichloride to give intermediate **C**, which then transforms to benzoxazole by simultaneous

presence of two benzoxazoles (in a ratio of ≈ 3 : 1) differing in chemical shifts for H-20, H-18, and H-19 resonances (see Experimental section, ***2.2.12. – 2.2.15.***). 2D ^{1}H NOESY NMR spectrum of crude compound **18a** unequivocally reveals that the major product is 17(20)*E*-benzoxazole, and the minor product is a related 17(20)*Z*- isomer (Figure 2). Similar patterns were observed in ^{1}H NMR spectra of benzoxazoles **8**, **9**, and **10**. Separation of crude benzoxazoles **18a**, **8**, **9** and **10** by preparative TLC allows to obtain pure 17(20)*E*-isomers **18a(*E*)**, **8(*E*)**, **9(*E*)** and **10(*E*)**. Removal of acetate protective group in compound **18(*E*)** gave benzoxazole **7(*E*).**

We tested compounds **3 – 10** as CYP17A1 inhibitors by sensitive electrochemical method, using the enzyme immobilized on a DDAB-modified electrode, according the assay reported earlier [19,20]. In the presence of oxygen and substrate (pregnenolone), decrease in catalytic current was observed, as shown by amperometric curve. Presence of inhibitors in the system led to reduced amperometric response.

Among new oxazolines, only compound **6** potently inhibited CYP17A1 activity. Under conditions used, compound **6** in a concentration of 1 μM caused 75.8% inhibition of CYP17A1 activity (Supplementary data, Fig. S-1). This value was close to related values for compounds **1** (78.6%, Supplementary data, Fig. S-2), **2** (53.9%) and abiraterone (56.3%) [19,20]. Compounds **3**, **4**, **5**, **7–10**, and galeterone in concentrations of 1 μM, 10 μM and 30 μM did not markedly inhibit CYP17A1 activity.

Previous docking studies revealed that *E*-isomer of compound **1** cannot form a stable complex with CYP17A1 active site in a manner identical to abiraterone [19]. X-Ray structure of abiraterone complex (3RUK) shows a direct coordinate bond between nitrogen atom of ligand and heme iron (distance 2.04Å). Equilibrium molecular dynamics (MD) simulations presented here confirm that the binding site configuration is unlikely to accommodate *E*-isomers of compounds **1** and **6** in such a manner for heme iron to form a direct coordinate bond to nitrogen or oxygen atom of oxazoline moiety. Nevertheless, differential UV absorption data indicate a change in high-spin/low-spin equilibrium compound **1** complex (data for compound **6** obtained to date was of insufficient quality, so not shown), which is usually deemed to originate from nitrogen-containing ligand replacing water molecule at the 6th heme coordinate position.

Studies conducted on other cytochromes with similar active sites suggest that it is rather

This binding mode, often identified as 'incomplete' binding, is characterized by smaller Soret band shift in UV spectrum. We observed the similar reduced (compared to abiraterone) shift for CYP17A1 complex with *E*-isomers of compound **1** [19]. This observation, combined with failure of computational docking to produce stable structures of these complexes, led us to the hypothesis that active site water might be involved, and an alternate type II interaction takes place.

To assess the possibility of such a water-bridged binding mode, for each complex we have built a pair of model structures: one with a water molecule placed at the heme 6th coordinate position (complexes C1w and C6w), and another with no such molecule (complexes C1 and C6). We also built a model for complex with abiraterone, to be used as reference. MD trajectories of 60 ns length revealed clear predominant structures in cases where water molecule was included, as well as in complex with abiraterone (Fig. 3).

We analyzed some important geometric parameters of ligand binding mode in model complexes (Supplementary data). In complexes C1w and C6w, average distance between nitrogen atom of oxazoline moiety (N), and the oxygen of water molecule at heme 6th coordinate position (OH), as well as angle between N, OH, and heme iron (Fe), were found to be nearly optimal for hydrogen bond formation (3.19Å and 125º in C1w; 2.92Å and 126º in C6w). This bond stability is confirmed by very low fluctuation of N-OH distances (Figure 4). From the Figure it is clear that in both C1w and C6w N-OH distances at points of peak density (2.89Å in C1w; 2.87Å in C6w; estimated from interpolated 2D histograms, see top-left inset on Figure 4) are lower than 3Å, and average distances presented above are slightly overestimated, because of temporary 'unbound' modes admixed in small fraction.

In C1w complex we also observed additional hydrogen bond between 6th coordinate water and Thr-306 located on I-helix (Figure 3B, Supplementary data, Fig. S-10). Both these bonds must significantly reduce active site water mobility (which was not directly observed in our MD simulations due to longer time scale of this process). On the contrary, with free heme 6th position in complexes C1 and C6, there was apparently no possibility to form any bond between nitrogen or oxygen moiety and heme iron, as N to Fe average interatomic distance well exceeded 4Å (Average N-Fe distances were 5.22Å in C1; 5.86Å in C6). Average angle between sulfur atom (S) of Cys-442, located on the exact opposite of 6th position in iron coordination sphere, Fe,

Data obtained by MD simulations, therefore, do not support the hypothesis taken by default in docking studies that *E*-isomers of $\Delta^{17(20)}$ compounds **1** and **6** are bound identically to abiraterone when forming complexes with CYP17A1 active site. Instead, as was shown by MD data presented here, the overall geometry of these compounds is favorable for formation of alternate, water-bridged complexes, with N-(H-bond)-OH-Fe connectivity, unlike in case of abiraterone, where direct N-Fe bond exists to support octahedral geometry of heme iron coordination sphere.

On the remote side (relative to heme), abiraterone is known to be anchored by hydrogen bond between 3-OH group and Asn-202 amide oxygen (calculated average donor-acceptor distance 2.79Å; Supplementary data, Fig. S-5). We observed the same bonding pattern in model complexes C1w and C1 (calculated average donor-acceptor distance 2.90 and 2.86Å, correspondingly; Figure 3, also see Supplementary data, Figs. S-10, S-19). On the contrary, compound **6** is lacking A ring of steroid moiety, but, instead, it carries a polar carbonyl group in ring B at position 5. This carbonyl group oxygen atom was found to be able to form a hydrogen bond with Arg-239 side-chain amino group in model complexes C6w and C6, which remained stable in course of simulation (calculated average donor-acceptor distance 2.92 and 2.75Å, correspondingly; Figure 3, also see Supplementary data, Figs. S-15, S-23). Therefore, according to our models, despite the lack of steroid ring A and hydroxyl group at position 3, which is capable of interaction with Asn-202, in complex of CYP17A1 with compound **6**, Arg-239 provides an equivalent remote-side anchor for the bound ligand.

inhibitory potency on structure of steroid moiety. Oxazolinyl and benzoxazolyl derivatives comprising 3β-hydroxy-5-ene fragments (**1** and **7**) were found to be potent inhibitors of prostate carcinoma cell growth, only slightly weaker than abiraterone and galeterone. Inhibitory potencies of 3-oxo-4-ene derivatives (**2** and **8**), and 5-oxo-seco-A derivatives (**6** and **10**) were significantly lower; compounds **3**, **4**, **5** and **9** slightly decreased growth of PC-3 and LNCaP cells.

Comparison of effects of oxazolinyl and benzoxazolyl derivatives comprising the same steroid moieties revealed that oxazolinyl derivatives were more potent inhibitors in PC-3 cells, while effects of the benzoxazolyl derivatives on PC-3 and LNCaP cells growth were less selective. These data also show that for [17(20)*E*]-21-norpregnene derivatives inhibition of PC-3 and LNCaP cells growth does not directly correlate to their ability to inhibit CYP17A1 activity. Oxazolines **1**, **2**, **6** potently inhibited CYP17A1 activity, while benzoxazoles **7**, **8**, **10** were not active, nevertheless the potency of these compounds to inhibit the growth of PC-3 and LNCaP cells was almost equivalent.

CONCLUSIONS.

Oxazolinyl derivatives of [17(20)*E*]-21-norpregnene comprising 3β-hydroxy-5-en- (**1**), 3-oxo-4-en- (**2**), and 5-oxo-4,5-seco-3-yn- (**6**) moieties efficiently inhibited CYP17A1 activity and prostate carcinoma PC-3 and LNCaP cells growth. Structural models of CYP17A1 complexes with 17(20)*E*- isomers of compounds **1** and **6**, built by molecular dynamics simulations, revealed that geometry of these compounds makes binding mode with water-bridged heme iron coordination preferential against the mode with direct nitrogen to iron bond, unlike in case with abiraterone. Benzoxazolyl derivatives (**7**, **8**, and **10**, respectively) were inactive toward CYP17A1, however, inhibited growth of PC-3 and LNCaP cells not less potently than oxazolines (**1**, **2**, and **6**).

ACKNOWLEDGEMENTS.

Authors are acknowledged to Maria G. Zavialova (from Orekhovich Institute of Biomedical Chemistry) for HRMS analysis. This study was supported by Russian Foundation for Basic Research (RFBR Grants №15-04-02939_a; №15-04-02426_a; №16-04-00293_a), State Academies of Sciences Fundamental Research Program for 2013–2020; and the Program ‘‘Molecular and cell biology” of the Presidium of RAS.

2. Hartmann RW, Ehmer PB, Haidar S, Hector M, Jose J, Klein CDP, et al. Inhibition of CYP 17, a new strategy for the treatment of prostate cancer. *Arch Pharm Med Chem* 2002;4:119–28.
3. Bruno RD, Njar VC. Targeting cytochrome P450 enzymes: a new approach in anti-cancer drug development. *Bioorg Med Chem* 2007;15:5047–60.
4. Baston E, Leroux FR. Inhibitors of steroidal cytochrome P450 enzymes as targets for drug development. *Rec Pat Anticancer Drug Disc* 2007;2:31–58.
5. Owen CP. 17α-Hydroxylase/17,20-lyase (P45017A1) inhibitors in the treatment of prostate cancer: *Anti-Cancer Agents Med Chem* 2009;*9*:613-626
6. Potter, G. A., Barrie, S. E., Jarman, M., Rowlands, M. G. Novel steroidal inhibitors of human cytochrome P45017alpha (17alpha-hydroxylase-C17,20-lyase): potential agents for the treatment of prostatic cancer. *J. Med. Chem.* 1995, *38,* 2463–2471.
7. Li R, Evaul K, Sharma KK, Chang K-H, Yoshimoto J, Liu J, Auchus RJ, Sharifi N. Abiraterone Inhibits 3b-Hydroxysteroid Dehydrogenase: A Rationale for Increasing Drug Exposure in Castration-Resistant Prostate Cancer. *Clin Cancer Res* 2012; 18; 3571–9.
8. Soifer HS, Souleimanian N, Wu S, Voskresenskiy AM, Collak FK, Cinar B, Stein CA. Direct regulation of androgen receptor activity by potent CYP17 inhibitors in prostate cancer cells. *J. Biol. Chem. 2012, 287:3777-3787.*
9. Richards J, Lim AC, Hay CW, Taylor AE, Wingate A, Nowakowska K, Pezaro C, Carreira S, Goodall J, Arlt W, *et al*: Interactions of abiraterone, eplerenone, and prednisolone with wild-type and mutant androgen receptor: A rationale for increasing abiraterone exposure or combining with MDV3100. *Cancer Res.* 2012, 72: 2176-82.
10. Grossebrummel H, Peter T, Mandelkow R, Weiss M, Muzzio D, Zimmermann U, Walther R, Jensen F, Knabbe C, Zygmunt M, Burchardt M, Stope MB. Cytochrome P450 17A1 inhibitor abiraterone attenuates cellular growth of prostate cancer cells independently from androgen receptor signaling by modulation of oncogenic and apoptotic pathways. *Int J Oncol*, 2016, 48: 793-800.
11. Handratta VD , Vasaitis TS, Njar VCO, Gediya LK, Kataria R, Chopra P, Newman D, Farquhar R, Guo Z, Qiu Y, Brodie AMH. Novel C-17-heteroaryl steroidal CYP17 inhibitors/antiandrogens: Synthesis, in vitro biological activity, pharmacokinetics, and

lyase inhibitor VN/124-1 inhibits growth of androgen-independent prostate cancer cells via induction of the endoplasmic reticulum stress response. *Mol Cancer Ther* 2008;7:2828-28362

14. Vasaitis T , Belosay A, Schayowitz A, Khandelwal A, Chopra P, Gediya LK, Guo Z, Fang H-B, Njar VCO, Brodie AMH. Androgen receptor inactivation contributes to antitumor efficacy of 17α-hydroxylase/17,20-lyase inhibitor 3β-hydroxy-17-(1H-benzimidazole-1-yl)androsta-5,16-diene in prostate cancer. *Mol Cancer Ther* 2008; 7:2348-2357.
15. Yu Z, Cai C, Gao S, Simon NI, Shen HC, Balk SP. Galeterone prevents androgen receptor binding to chromatin and enhances degradation of mutant androgen receptor. *Clin Cancer Res*. 2014; 20: 4075–4085
16. Ajdukovic JJ, Djurendic EA, Petri ET, Klisuric OR, Celic AS, Sakac MN, et al., 17(*E*)-Picolinylidene androstane derivatives as potential inhibitors of prostate cancer cell growth: antiproliferative activity and molecular docking studies. *Bioorg Med Chem* 2013; 21: 7257– 66.
17. Szabó N, Ajdukovic J, Djurendic E, Sakač M, Ignáth I, et. al., Determination of 17α-hydroxylase-C17,20-lyase (P45017α) enzyme activities and their inhibition by selected steroidal picolyl and picolinylidene compounds. *Acta Biologica Hungarica* 2015; 66: 41–51.
18. Jakimov DS, Kojic VV, Aleksic LD, Bogdanovic GM, Ajdukovic JJ, Djurendic EA, Penov Gaši KM, Sakac MN, Jovanovic´-Šanta SS. Androstane derivatives induce apoptotic death in MDA-MB-231 breast cancer cells. *Bioorg Med Chem*, 2015, 23, 7189–7198
19. Kuzikov AV, Dugin NO, Stulov SV, Shcherbinin DS, Zharkova MS, et. al., Novel oxazolinyl derivatives of pregna-5,17(20)-diene as 17a-hydroxylase/17,20-lyase (CYP17A1) inhibitors. *Steroids* 2014; 88: 66–71.
20. Kostin VA, Zolottsev VA, Kuzikov AV, Masamrekh RA, Shumyantseva VV, Veselovsky AV, Stulov SV, Novikov RA, Timofeev VP, Misharin AY. Oxazolinyl derivatives of [17(20)*E*]-21-norpregnne differing in the structure of A and B rings. Facile synthesis and inhibition of Cyp17A1 catalytic activity. *Steroids* 2016;115:114-122

2011;32:2359–2368. doi:10.1002/jcc.21816.

23. Shahrokh K, Orendt A, Yost G, Cheatham T. Quantum mechanically derived AMBER-compatible heme parameters for various states of the cytochrome P450 catalytic cycle. *J Comput Chem.* 2012;33:119–133. doi:10.1002/jcc.21922.
24. Humphrey W, Dalke A, Schulten K. VMD: Visual molecular dynamics. *Journal of Molecular Graphics*. 1996;14:33–38. doi:10.1016/0263-7855(96)00018-5.
25. Phillips JC, Braun R, Wang W, Gumbart J, Tajkhorshid E, Villa E, Chipot C, Skeel RD, Kalé L, Schulten K. Scalable molecular dynamics with NAMD. *Journal of Computational Chemistry*. 2005;26:1781–1802. doi:10.1002/jcc.20289.
26. Hunter JD. Matplotlib: A 2D Graphics Environment. *Computing in Science Engineering*. 2007;9:90–95. doi:10.1109/MCSE.2007.55.
27. Oliphant TE. Python for Scientific Computing. *Computing in Science Engineering*. 2007;9:10–20. doi:10.1109/MCSE.2007.58.
28. Mosmann T. Rapid colorimetric assay for cellular growth and survival: application to proliferation and cytotoxicity assays. *J. Immunol. Meth.*, 1983; *65*: 55-63
29. Vorbruggen H, Krolikiewicz K, A simple synthesis of 2-oxazolines, 2-oxazines, 2-thiazolines and 2-imidazolines, *Tetrahedron Lett.* 1981; 45: 4471–4474.
30. Vorbruggen H, Krolikiewicz K, A simple synthesis of 2-oxazolines, 2-oxazines, 2-thiazolines and 2-substituted benzoxazoles, *Tetrahedron* 1993; 49: 9353–9372.
31. Conner KP, Woods C, Atkins WM. Interactions of Cytochrome P450s with their Ligands. *Arch Biochem Biophys.* 2011:50756–65. doi:10.1016/j.abb.2010.10.006.
32. Seward HE, Roujeinikova A, McLean KJ, Munro AW, Leys D. Crystal Structure of the Mycobacterium tuberculosis P450 CYP121-Fluconazole Complex Reveals New Azole Drug-P450 Binding Mode. *J. Biol. Chem.* 2006;281:39437–39443. doi:10.1074/jbc.M607665200.

INCUBATION

Compound	GI_{50}, μM	
	PC-3	LNCaP
1	**11.0**	**14.8**
2	**14.1**	**24.3**
3	**28.0**	**43.5**
4	**>50**	**>50**
5	**39.0**	**>50**
6	**15.9**	**32.1**
7	**11.2**	**7.9**
8	**14.0**	**23.9**
9	**>50**	**38.0**
10	**11.1**	**19.0**
Abiraterone	**8.7**	**23.0**
Galeterone	**7.1**	**4.2**

CCl_4 / CH_3CN, 2°C, 90 min, then $H_2N(CH_2)_2OH$, $(CH_3CH_2)_3N$, 2°C→20°C, 2 h; *d* – CH_3OH, p-TSA, reflux, 1 h; *d* – 1M HCl / tetrahydrofurane, r. t., 2h.

Scheme 2. *a* –H_2O_2, NaOH / CH_3OH - H_2O, 2°C, 18 h; *b* – *p*-$TsNHNH_2$ / CH_2Cl_2 - CH_3COOH, r. t., 3h; *c* – NaOH / *i*-PrOH, reflux, 3h; *d* – Ph_3P, CCl_4 / CH_3CN, 2°C, 90 min, then $H_2N(CH_2)_2OH$, $(CH_3CH_2)_3N$, 2°C→20°C, 2 h.

Scheme 3. *a* – Ph_3P, CCl_4 / CH_3CN, 2°C, 90 min; *b* – *o*-$H_2N(C_6H_4)OH$, Py, 2°C→20°C, 30 min; *c* – Ph_3P, CCl_4 / CH_3CN, Py, 50°C, 3 h; *d* – isolation of 17(20)*E*-isomer; *e* – K_2CO_3 / CH_3OH - H_2O, reflux, 30 min.

Scheme 4. The proposed scheme for formation of benzoxazole derivatives of 17(20)-norpregnene.

Fig. 2. Fragment of 2D NOESY ^{1}H NMR spectrum of isolated mixture of (*E*)- and (*Z*)- 2'-[(3β-acetoxyandrost-5-en-17-ylidene)methyl]-benzo-[d]-oxazoles **18a**.

Fig. 3 Ligand binding modes in model CYP17A1/abiraterone complex (A), and water-bridged model complexes of CYP17A1 with compounds 1 (B, complex C1w), and 6 (C and D, two views of complex C6w active site). Structures presented here correspond to average values (A), or, in cases when average was significantly biased by additional minor mode, estimated probability density function maxima (B-D), of binding mode key geometric parameters (for details see text).

Fig. 4 Geometric parameters fluctuations in model water-bridged complexes of CYP17A1 with compounds **1** and **6**: C1w (A), and C6w (B), calculated from MD trajectories. Densely packed points indicate stable binding mode. Vertical axis of 2D plot: distance between oxazoline nitrogen atom and heme iron. Horizontal axis of 2D plot: angle formed by oxazoline nitrogen, coordinated water oxygen, and heme iron. Each point on 2D plot corresponds to single MD frame, sampled every 8ps. Green mark denotes the average value, and red mark – the peak maximum of estimated probability density function (PDF). Estimated PDFs are shown on small insets on top-left corners. Histograms level units are frame counts.

Fig. 5 Geometric parameters fluctuations in model complexes of CYP17A1 with compounds **1** and **6**: C1 (A), and C6 (B), calculated from MD trajectories. Loosely packed points indicate that no stable binding mode can be predicted from the simulation. Vertical axis of 2D plot: distance between oxazoline nitrogen atom and heme iron. Horizontal axis of 2D plot: angle formed by oxazoline nitrogen, heme iron, and CYS388 sulfur atom. Each point on 2D plot corresponds to single MD frame, sampled every 8ps. Green mark denotes the average value, and red mark – the maximum peak of estimated probability density function (PDF). Estimated PDFs are shown on small insets on top-left corners. Histograms level units are frame counts.

3. Computational modeling of [17(20)*E*]-21-norpregnene oxazolinyl derivatives binding modes in CYP17A1 active site
4. Inhibition of prostate carcinoma PC-3 and LNCaP cells growth.

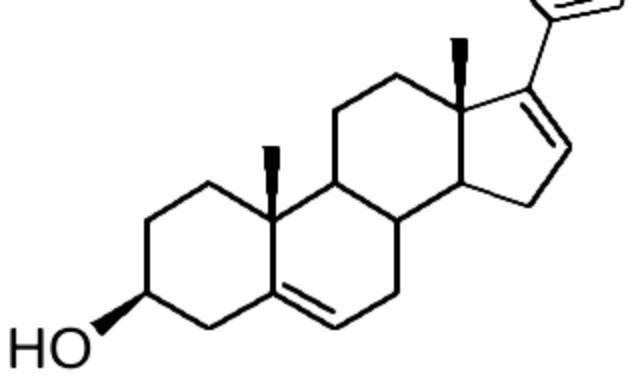

abiraterone

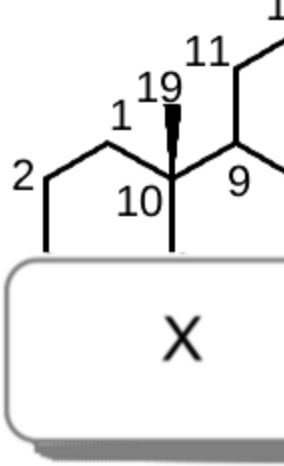

1 - 6

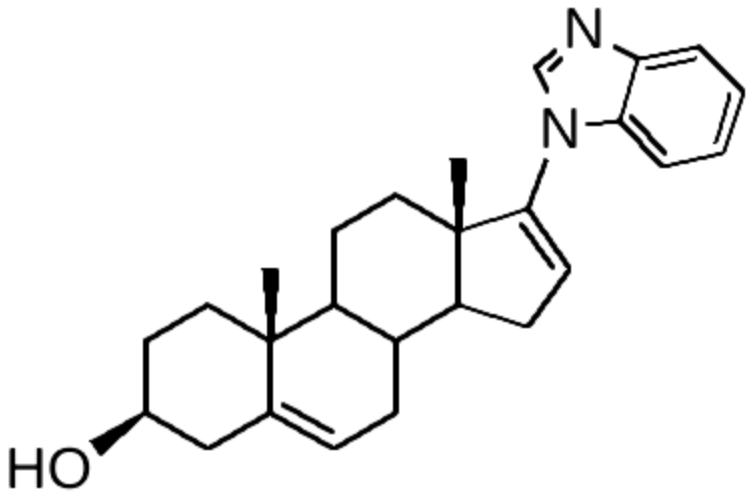

galeterone

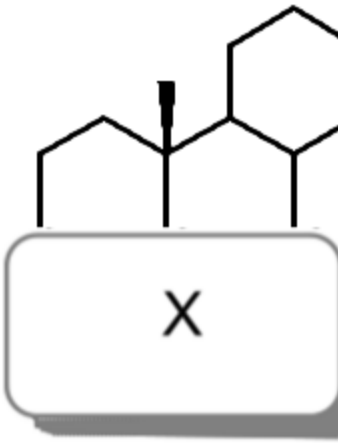

7 - 10

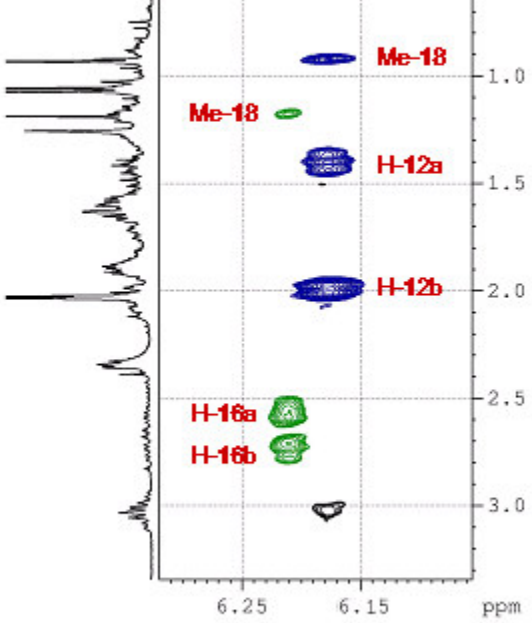

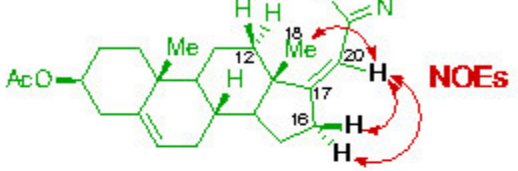

Z- (minor)

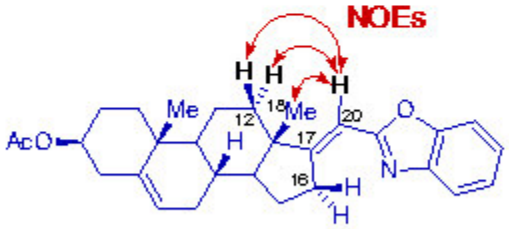

E- (major)

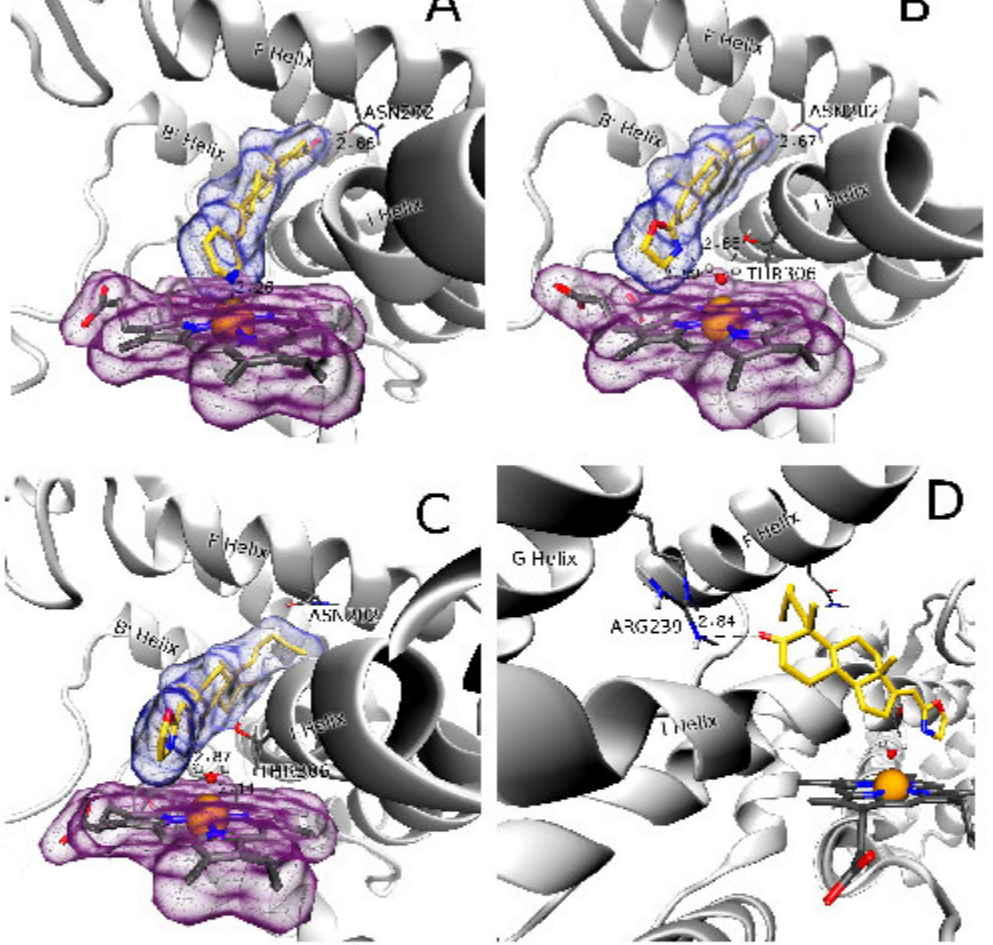
A
F Helix
B' Helix
ASN202
2.86
I Helix
2.28
B
F Helix
B' Helix
ASN202
2.67
I Helix
THR306
C
F Helix
B' Helix
ASN202
I Helix
2.87
THR306
D
G Helix
F Helix
ARG230
2.84
I Helix

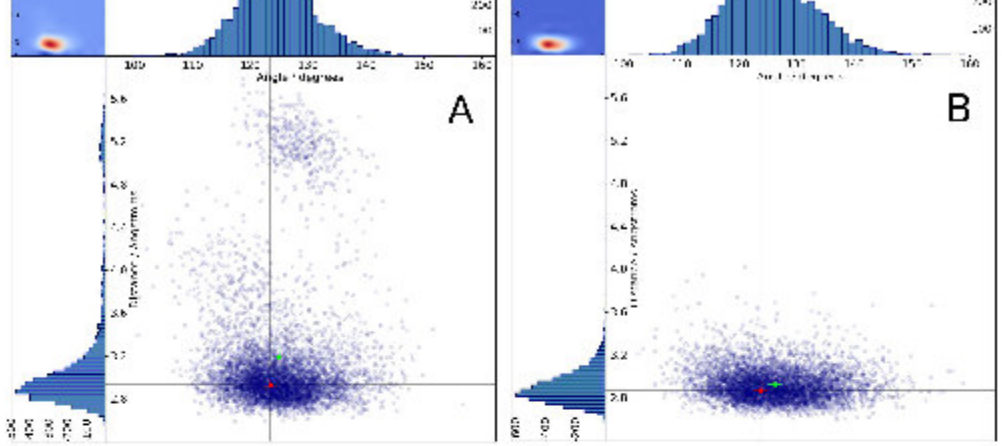

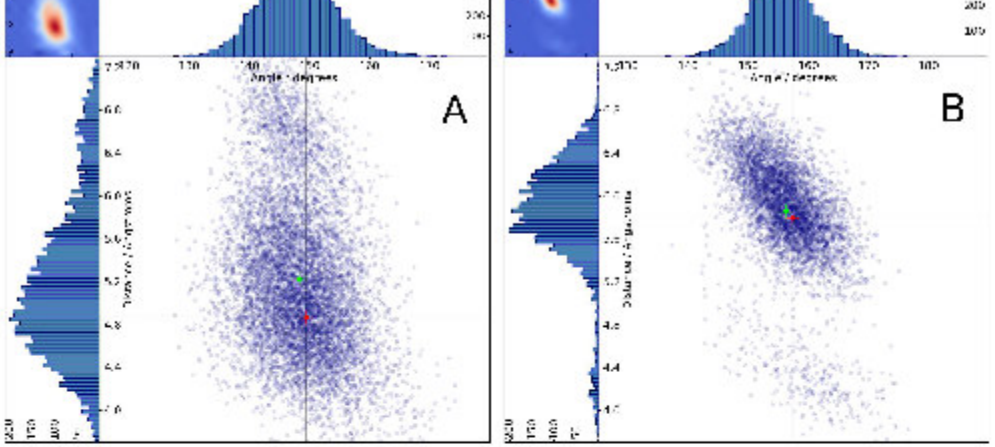

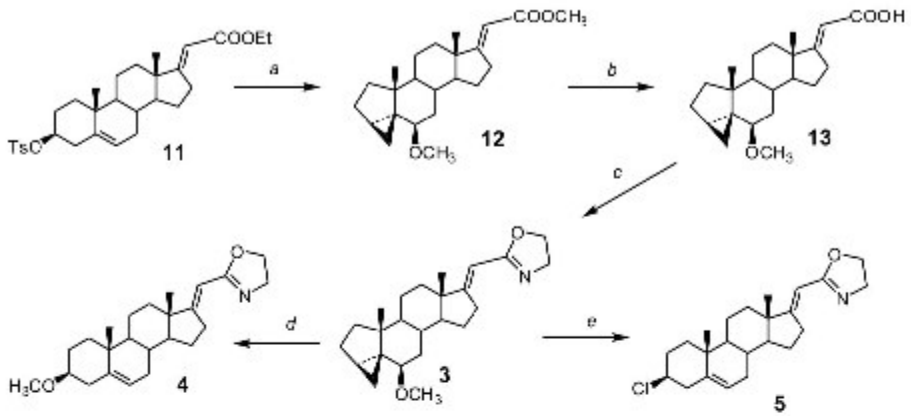
COOEt
a
COOCH3
b
COOH
TsO
11
OCH3
12
OCH3
13
c
O
N
H3CO
4
d
OCH3
3
e
Cl
5

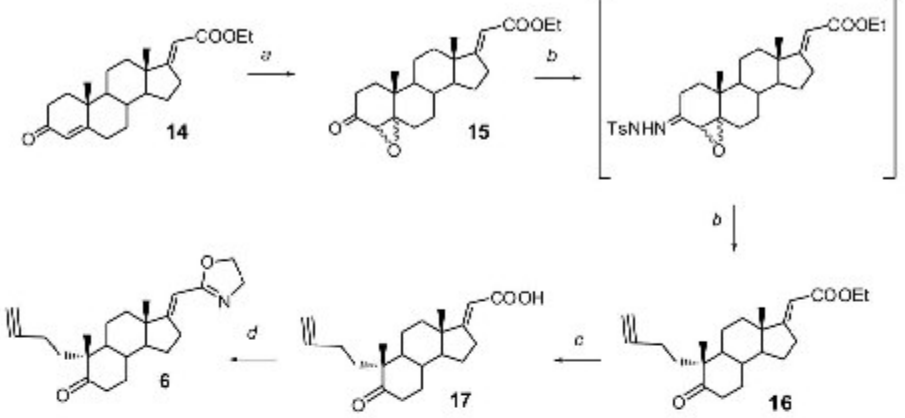

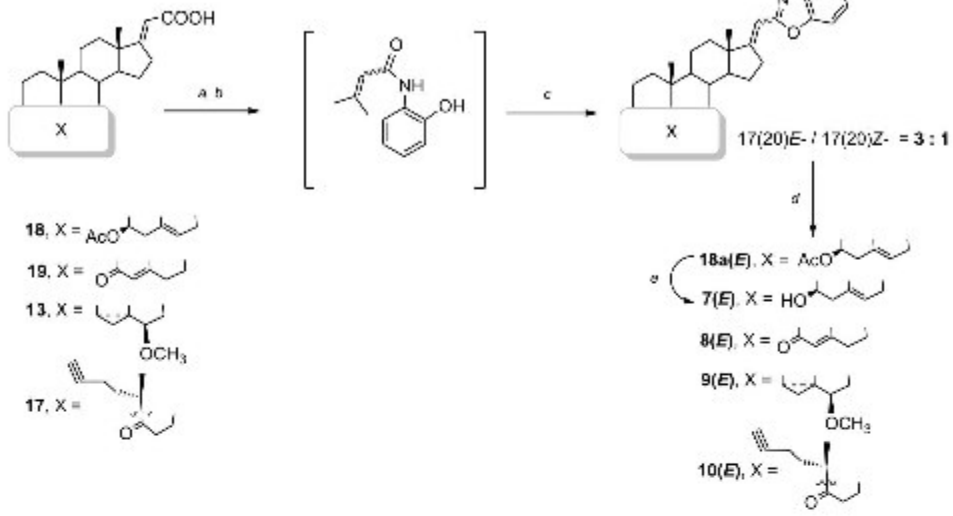
COOH
X
a, b
NH
OH
c
X
17(20)E- / 17(20)Z- = 3 : 1
d
18, X = AcO
19, X =
13, X =
OCH3
17, X =
18a(E), X = AcO
e
7(E), X = HO
8(E), X =
9(E), X =
OCH3
10(E), X =